


Correlated electronic structure, orbital-selective behavior, and magnetic correlations in double-layer $\text{La}_3\text{Ni}_2\text{O}_7$ under pressure

D. A. Shilenko¹ and I. V. Leonov^{1,2}¹*Institute of Physics and Technology, Ural Federal University, 620002 Yekaterinburg, Russia*²*M. N. Miheev Institute of Metal Physics, Russian Academy of Sciences, 620108 Yekaterinburg, Russia*
 (Received 29 June 2023; revised 31 July 2023; accepted 22 August 2023; published 5 September 2023)

Using *ab initio* band structure and DFT + dynamical mean-field theory methods we examine the effects of electron-electron interactions on the normal state electronic structure, Fermi surface, and magnetic correlations of the recently discovered double-layer perovskite superconductor $\text{La}_3\text{Ni}_2\text{O}_7$ under pressure. Our results suggest the formation of a negative charge transfer mixed-valence state with the Ni valence close to 1.75+. We find a remarkable orbital-selective renormalization of the Ni 3*d* bands, with $m^*/m \sim 3$ and 2.3 for the Ni $3z^2-r^2$ and x^2-y^2 orbitals, respectively, in agreement with experimental estimates. Our results for the *k*-dependent spectral functions and Fermi surfaces show significant incoherence of the Ni $3z^2-r^2$ states, implying the proximity of the Ni 3*d* states to orbital-dependent localization. Based on our analysis of the static magnetic susceptibility, we propose the possible formation of the spin and charge (or bond) density wave stripe states in high-pressure $\text{La}_3\text{Ni}_2\text{O}_7$.

DOI: [10.1103/PhysRevB.108.125105](https://doi.org/10.1103/PhysRevB.108.125105)

I. INTRODUCTION

The recent discovery of superconductivity in the hole-doped infinite-layer nickelate thin films $R\text{NiO}_2$ ($R = \text{La, Nd, Pr, Sr, Ca}$) [1–10] has stimulated intensive efforts in understanding of the electronic structure, magnetic properties, and microscopic mechanisms of the high- T_c superconductivity in nickelates [11–15]. Upon various chemical compositions, epitaxial lattice strain and pressure superconductivity in infinite-layer $R\text{NiO}_2$ films appears below $T_c \sim 31$ K. In $R\text{NiO}_2$, Ni ions adopt a nominal $\text{Ni}^+ 3d^9$ configuration (with the planar Ni x^2-y^2 orbital states dominated near the Fermi level) [16–18], being isoelectronic to Cu^{2+} in the parent hole-doped superconductor CaCuO_2 with a critical temperature ~ 110 K [19–21]. However, it has been shown that the low-energy states of $R\text{NiO}_2$ differ significantly from those of the hole-doped CaCuO_2 . In fact, in $R\text{NiO}_2$ the Ni x^2-y^2 states experience strong hybridization with the rare-earth 5*d* orbitals, resulting in self-doping (with the 5*d* bands crossing the Fermi level) and noncupratelike multiorbital Fermi surface (FS) [22–41].

Moreover, recent experiments (resonant inelastic x-ray scattering, RIXS) provide evidence for the existence of sizable antiferromagnetic correlations (with no static magnetic order) [42–45]. In addition, based on the resonant diffraction at the Ni L_3 edge, the authors propose the formation of translational symmetry broken states (charge density wave stripes) [46–51]. All these imply the importance of strong electronic correlations in infinite-layer $R\text{NiO}_2$ [52,53]. In agreement with this, applications of the DFT + dynamical mean-field theory (DFT + DMFT) [54,55] and GW+DMFT [56,57] electronic structure calculations show a remarkable orbital-dependent localization of the Ni 3*d* states, complicated by large hybridization with the rare-earth 5*d* states [22–41].

So far, superconductivity has been observed in the epitaxial thin films of the hole-doped nickelates $R\text{NiO}_2$ and (undoped) quintuple-layer square-planar nickelate $\text{Nd}_6\text{Ni}_5\text{O}_{12}$ systems synthesized using soft-chemical topotactic reduction of the parent perovskite compounds (with metal hydrides). Interestingly, superconductivity sets in the thin films nickelates with the Ni ions in a mixed-valence average state near to $\text{Ni}^{1.2+}$ [1–10]. However, no evidence of superconductivity has been observed in the bulk samples [58–60], while magnetic susceptibility measurements of bulk $R\text{NiO}_2$ (with $R = \text{La, Pr, and Nd}$) show universal spin-glass behavior at low temperatures [44]. This suggests the crucial role of hydrogen for superconductivity in the infinite-layer nickelates [61,62].

In this respect, the recently reported by Sun *et al.* superconductivity in the (bulk hydrogen free) single crystal double-layer perovskite $\text{La}_3\text{Ni}_2\text{O}_7$ with a high critical temperature ~ 80 K under pressure between $\sim 14 - 43$ GPa [63,64] has stimulated intensive efforts in understanding of its electronic structure [65–70]. In contrast to the infinite-layer nickelates in $\text{La}_3\text{Ni}_2\text{O}_7$ (LNO), the Ni ions adopt a nominal mixed-valence $\text{Ni}^{2.5+} (3d^{7.5})$ electron configuration. Under pressure, LNO undergoes a structural transition from the low-pressure *Amam* to orthorhombic *Fmmm* phase above ~ 15 GPa, which is characterized by a change of the bond angle of Ni-O-Ni (to 180° along the *c* axis, with no tilting of oxygen octahedra) [63,64]. Superconductivity in the high-pressure *Fmmm* phase of LNO is found to compete with a strange (bad) metal phase above T_c and weakly insulating behavior at pressures below 15 GPa.

Moreover, in recent experiments (resistance, magnetization, Raman scattering, and specific heat measurements) LNO is found to show anomaly in the transport properties near 153 K (at ambient pressure), suggesting the formation of spin and charge density wave states [64]. These experiments

also show the importance of effective mass renormalizations caused by correlation effects, implying the significance of electron-electron interactions in LNO. While the electronic state of the high-pressure (HP) phase of LNO has recently been discussed using various band-structure, GW, DFT + DMFT, and GW+DMFT methods [65–70], its properties are still poorly understood. The fundamental question concerning the mechanism of superconductivity and the impact of electronic correlations on superconductivity and magnetism in nickelates remains a subject of intense debates [65–78].

We address this topic in our present study. In our work, we explore the effects of correlations on the electronic structure and magnetic state of the normal state of the recently discovered double-layer nickelate superconductor $\text{La}_3\text{Ni}_2\text{O}_7$ under pressure [63,64]. In particular, we use the DFT + DMFT approach [79–81] to study the electronic structure, orbital-dependent correlation effects, Fermi surface topology, and magnetic correlations in LNO. Our results reveal a remarkable orbital-selective renormalizations of the Ni $3d$ states. Our analysis of the k -resolved spectral functions and correlated Fermi surfaces suggests significant incoherence of the electronic Ni $3z^2-r^2$ states, implying the proximity of the Ni e_g states to orbital-selective localization. Our results propose the possible formation of spin and charge (or bond) density wave stripe states, which seems to be important for understanding of the anomalous properties of LNO.

II. RESULTS AND DISCUSSION

A. Electronic structure

We start by computing the electronic structure and analysis of the orbital-selective behavior of the Ni $3d$ states. We perform the nonmagnetic DFT band structure calculations (within generalized gradient approximation with Perdew-Burke-Ernzerhof exchange functional) [82] as implemented in the Quantum ESPRESSO package [83,84] using ultrasoft pseudopotentials [85,86]. In our calculations we use the experimentally refined crystal structure (at about 29.5 GPa) and preform structural optimization of atomic positions with fixed lattice constants a , b , and c . Our DFT results are in overall agreement with those in Refs. [65–69]. Thus, the partially occupied bands crossing the Fermi level are of Ni e_g character with strong hybridization with the O $2p$ states. We note that the DFT Ni e_g bandwidth is about 4.7 and 3.8 eV for the Ni x^2-y^2 and $3z^2-r^2$ orbitals, respectively, while the crystal field splitting between these orbitals is ~ 0.3 eV (for LNO at about 29.5 GPa). It is worth noting that at ambient pressure the bandwidth of the Ni x^2-y^2 and $3z^2-r^2$ orbitals is about 4.2 and 3.3 eV, respectively; the crystal field splitting between these orbitals is ~ 0.3 eV.

The Ni t_{2g} states are fully occupied and appear at about -0.5 eV below the Fermi level. The occupied part of the O $2p$ bands appears at -8.5 to -2 eV below the Fermi level. In agreement with previous results, our DFT estimate of the charge-transfer energy difference $\Delta \equiv \epsilon_d - \epsilon_p \sim 3.8$ eV [87,88] is remarkably smaller than that typical for the infinite-layer nickelates ~ 4.2 eV [1–15]. This implies the importance of charge transfer effects in LNO, while the infinite-layer nickelates are in fact closer to a Mott-Hubbard

regime [2,5,11–15]. The bands originating from the La $5d$ states are unoccupied and appear at about 2 eV above E_F .

We note however that for LNO with the experimental (unrelaxed) crystal structure, the La $5d$ states cross the Fermi level near the Γ point of the Brillouin zone (BZ). Our results for the unrelaxed LNO are summarized in the Supplemental Material [89]. This behavior results in self-doping, i.e., in charge transfer between the Ni e_g and La $5d$ states similar to that in RNiO_2 . We note that in RNiO_2 the rare-earth $5d$ states cross the Fermi level near the Γ and A points of the BZ, resulting in the appearance of three dimensional FS pockets. Moreover, structural optimization within DFT results in a remarkable upshift of the La $5d$ states by about 1–2 eV above the E_F . As a result, the Fermi surface of the HP LNO (with optimized structure) consists of two electron pockets with mixed Ni x^2-y^2 and $3z^2-r^2$ character, centered at the Γ and M points of the BZ—a quasi-two-dimensional cylinderlike FS at the Γ point, with small warping along the c axis, and a more squaredlike FS at the M point—and one hole pocket due to the Ni $3z^2-r^2$ states at the M point. On the other hand, our DFT calculations for LNO with the experimental structure give an additional quasi-2D cylinderlike electron FS of the La $5d$ character at the Γ point, with substantial variation of the FS cross section along the c axis (see Fig. S1 of the Supplemental Material).

B. Effects of correlations on the electronic structure

Next, we discuss the effects of electronic correlations on the electronic structure, Fermi surface, and magnetic properties of LNO under pressure. In order to treat correlation effects in the partially filled Ni $3d$ states (La $5d$ states are more extended, located above E_F , and to a large extent can be considered as uncorrelated) we employ the DFT + DMFT method [54,55]. We use a fully charged self-consistent DFT + DMFT implementation [79–81] with plane-wave pseudopotentials [83,84] to compute the orbital dependent and k -resolved spectral functions of paramagnetic (PM) LNO. In these calculations we neglect the possible appearance of spin and charge density wave states in LNO [46–50,90–100]. For the low energy states we construct a basis set of atomic-centered Wannier functions for the Ni $3d$, La $5d$, and O $2p$ valence states using the energy window spanned by these bands [101,102]. This allows us to treat the electron-electron interactions in the partially filled Ni $3d$ shell, complicated by a charge transfer between the Ni $3d$, O $2p$, and La $5d$ states (the O $2p$ and La $5d$ states are treated as uncorrelated on the DFT level within the fully charge self-consistent DFT + DMFT method).

In our DFT + DMFT calculations we employ the continuous-time hybridization expansion quantum Monte Carlo algorithm in order to solve a realistic many-body problem describing the strongly correlated Ni $3d$ electrons in LNO [103]. We use the segment implementation of CT-QMC, in which by construction the pair and spin-flip hopping terms of the Hund's exchange are neglected. In agreement with previous applications of DFT + DMFT, to study infinite-layer and perovskite nickelates [22,22–41] we take the Hubbard $U = 6$ eV, Hund's exchange $J = 0.95$ eV, and the fully localized double-counting correction (evaluated from

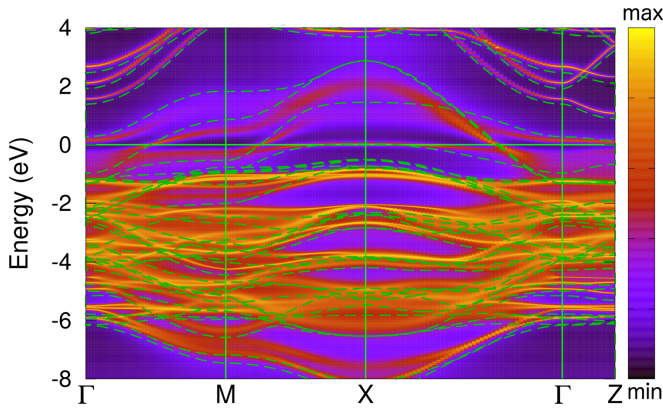


FIG. 1. k -resolved spectral functions of PM $\text{La}_3\text{Ni}_2\text{O}_7$ calculated using DFT + DMFT at $T = 290$ K. The calculations are performed for the orthorhombic $Fmmm$ structure taken at about 29.5 GPa with optimized atomic positions. The DFT + DMFT spectral functions are compared with the nonmagnetic DFT results (shown with green broken lines).

the self-consistently determined local occupations) [104]. In our calculations we neglect the spin-orbit coupling. In order to compute the k -resolved spectra and correlated Fermi surfaces we perform analytic continuation of the self-energy results using Padé approximants. Our DFT + DMFT calculations are performed for the normal state of PM LNO at a temperature $T = 290$ K. All the details concerning the DFT + DMFT method employed in the present study can be found in Ref. [81] (and references therein).

In Fig. 1 we display our results for k -resolved spectral functions of LNO with the optimized atomic positions obtained using DFT + DMFT (in comparison to the nonmagnetic DFT results). The orbital-dependent spectral functions are shown in Fig. 2. The DFT + DMFT results for LNO with the experimental lattice are shown in Figs. S1 and S2 in the SM. Overall, our DFT + DMFT results agree well with those published previously [66,67]. Our calculations show the mixed Ni x^2-y^2

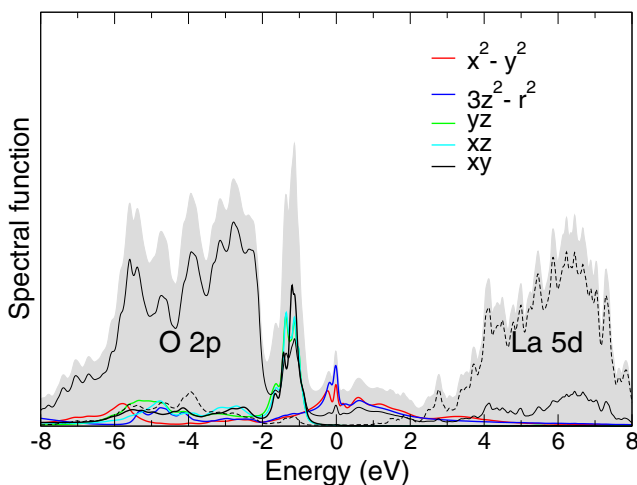


FIG. 2. Orbital-dependent spectral functions of PM $\text{La}_3\text{Ni}_2\text{O}_7$ as obtained by DFT + DMFT at $T = 290$ K. The Ni $3d$ states are magnified by a factor two for better readability.

and $3z^2-r^2$ states crossing the Fermi level. The occupied O $2p$ states located at -8.5 to -1.9 eV below E_F , with strong hybridization with the partially occupied Ni $3d$ states. The Wannier Ni x^2-y^2 and $3z^2-r^2$ orbital occupations are close to half-filling, of ~ 0.54 and 0.6 per spin orbit, respectively. This is in remarkable contrast to that for the optimally doped RNiO_2 where the Ni $3z^2-r^2$ orbital occupancy is considerably larger, ~ 0.85 [22–41]. The total Wannier Ni $3d$ occupation is about 8.24. Moreover, our analysis of the weights of different atomic configurations of the Ni $3d$ electrons (in DMFT the Ni $3d$ electrons are seen fluctuating between various atomic configurations) gives 0.1, 0.55, and 0.32 for the d^7 , d^8 , and d^9 configurations, respectively, in accordance with the mixed-valence Ni $3d^8$ and $3d^9$ configurations of the Ni ions. Our analysis gives a formal valence state of $1.75+$ for the Ni ions which significantly differ from $\text{Ni}^{2.5+}$. Our results therefore suggest that LNO appears close to a negative charge transfer regime [105,106] (similarly with the charge-transfer state in superconducting cuprates), in contrast to the infinite-layer nickelates. The latter are in fact close to a Mott-Hubbard regime [2,5,11–15]. Moreover, our estimate for the spin-state configuration gives 0.65 and 0.35 for the high-spin and low-spin state configurations, respectively. This suggests strong interplay of the $S = 0$ and $S = 1/2$ states in the electronic structure of LNO (the corresponding weights are 0.23, 0.32, and 0.32 for the $3d^8 S = 0$, $3d^8 S = 1$, and $3d^9 S = 1/2$ spin configurations, respectively), similarly to that in RNiO_2 [34].

C. Orbital-selective behavior

The electron bands originating from the La $5d$ states are unoccupied and appear at 2.2 eV above E_F . Overall, the physical picture remains similar to that obtained within DFT, complicated by a remarkable renormalization of the Ni $3d$ states and their substantial orbital-selective incoherence (bad-metal behavior) caused by correlation effects. In fact, the electronic structure of LNO is characterized by a Fermi-liquid-like behavior of the Ni $3d$ self-energies [see Figs. 3(a) and 3(b)], with a substantial orbital-dependent quasiparticle damping of $\text{Im}[\Sigma(i\omega)] \sim 0.18$ and 0.25 eV for the Ni x^2-y^2 and $3z^2-r^2$ quasiparticle states at the first Matsubara frequency, at $T = 290$ K. The Ni t_{2g} states are sufficiently coherent, with $\text{Im}[\Sigma(i\omega)]$ below 0.02 eV at the first Matsubara frequency. Using Padé extrapolation of the self-energy $\Sigma(i\omega)$ to $i\omega \rightarrow 0$ we obtain 0.08 and 0.11 eV for the Ni x^2-y^2 and $3z^2-r^2$ states at the Fermi energy, respectively.

Moreover, our DFT + DMFT calculations reveal a remarkable orbital-selective renormalization of the partially occupied Ni $3d$ bands. Our analysis of the orbitally resolved quasiparticle mass enhancement evaluated as $\frac{m^*}{m} = [1 - \partial \text{Im}[\Sigma(i\omega)] / \partial i\omega]_{i\omega \rightarrow 0}$ using Padé approximants gives 2.3 and 3 for the Ni x^2-y^2 and $3z^2-r^2$ bands, respectively. The effective mass enhancements of the Ni t_{2g} states is much weaker, of ~ 1.3 . That is, the Ni $3z^2-r^2$ states are seen to be more correlated and incoherentlike than the in-plane Ni x^2-y^2 orbitals. This result is consistent with a narrower DFT bandwidth of the Ni $3z^2-r^2$ orbitals which is by $\sim 19\%$ less than that for the x^2-y^2 states. Our result for the quasiparticle mass enhancement is in agreement with experimental estimates from transport measurements for single crystals of

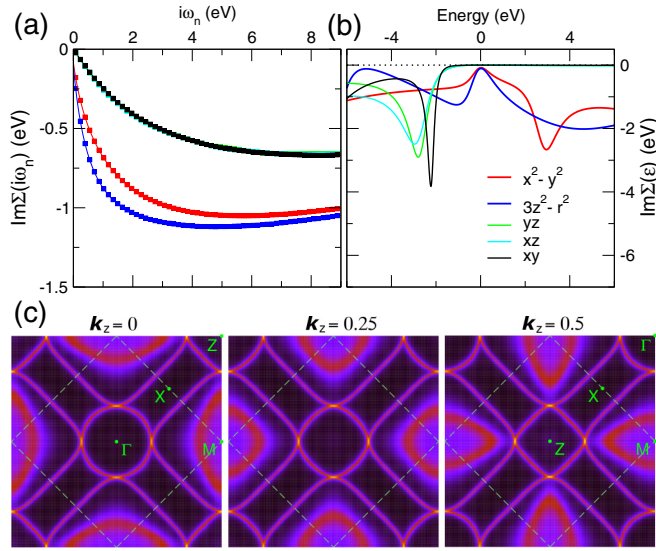


FIG. 3. Orbital-dependent imaginary part of the Ni $3d$ self-energies $\text{Im}[\Sigma(i\omega)]$ on the Matsubara axis (a), the imaginary part of the analytically continued Ni $3d$ self-energies $\text{Im}[\Sigma(\omega)]$ on the real energy axis [109] (b), and correlated Fermi surfaces [spectral function $A(\mathbf{k}, \omega)$ evaluated at $\omega = 0$] for different k_z (c) for HP $\text{La}_3\text{Ni}_2\text{O}_7$ calculated by DFT + DMFT at $T = 290$ K.

the double-layer LNO and three-layer $\text{La}_4\text{Ni}_3\text{O}_{10}$, ~ 2.12 and 2.56 , respectively [64]. We also note that the effective mass enhancement of the Ni $3d$ states depends sensitively upon variation of the Hubbard U and Hund's J coupling values. Thus, for $U = 4$ eV and $J = 0.45$ eV we obtain $m^*/m \sim 1.4$ and 1.5 for the Ni x^2-y^2 and $3z^2-r^2$ orbitals, respectively. For $U = 6$ eV and $J = 0.45$ eV we find ~ 1.6 and 1.9 , and for $U = 4$ eV and $J = 0.95$ eV we find ~ 1.7 and 2.1 , respectively. That is, it reveals a strong sensitivity to changes of the Hund's J , while dependence of m^*/m on the U value is much weaker. This result is in overall agreement with the results presented in Ref. [71]. In agreement with our results, the DFT + DMFT calculations with a remarkably larger Hubbard $U = 10$ eV and Hund's exchange $J = 1$ eV give $m^*/m \sim 5.6$ and 6.5 for the Ni x^2-y^2 and $3z^2-r^2$ orbitals, respectively [66].

This behavior is also consistent with our analysis of the orbital-dependent local spin susceptibility $\chi(\tau) = \langle \hat{m}_z(\tau) \hat{m}_z(0) \rangle$, evaluated within DMFT (see Fig. 4). Thus, our result suggests the proximity of both the Ni x^2-y^2 and $3z^2-r^2$ states to localization. While the Ni $3z^2-r^2$ orbitals show a slow decaying behavior of $\chi(\tau)$ to $0.06 \mu_B^2$ at $\tau = \beta/2$, for the Ni x^2-y^2 states it is remarkably smaller, $\sim 0.03 \mu_B^2$. Our results therefore suggest that magnetic correlations in LNO are at the verge of an orbital-dependent formation of local magnetic moments, suggestive of Hund's metal behavior [107,108]. In agreement with this, the calculated (instantaneous) magnetic moment of Ni is about $1.3 \mu_B$, which is consistent with a nearly $S = 1/2$ state of nickel. At the same time, the fluctuating moment evaluated as $\mu \equiv [k_B T \int \chi(\tau) d\tau]^{1/2}$ is significantly smaller, $0.55 \mu_B$. It is interesting to mention that our DFT + DMFT calculations for LNO with the experimental structure give similar estimates of $m^*/m \sim 2.2$ and 2.5 , for the Ni x^2-y^2 and $3z^2-r^2$ orbitals at $T = 290$ K, respectively.

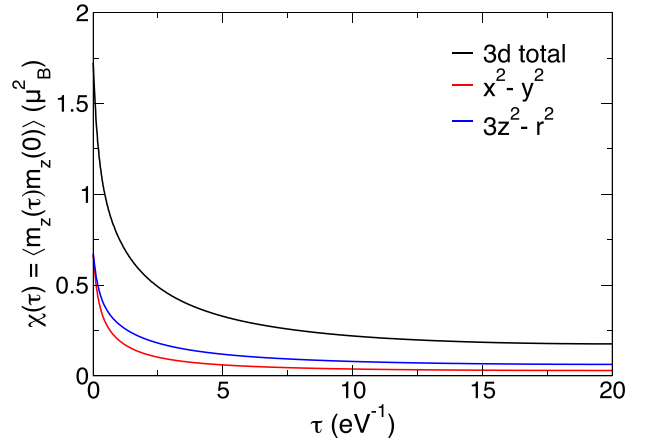


FIG. 4. Orbital-resolved local spin correlation functions $\chi(\tau) = \langle \hat{m}_z(\tau) \hat{m}_z(0) \rangle$ as a function of the imaginary time τ for the Ni $3d$ orbitals calculated by DFT + DMFT for the high-pressure PM $\text{La}_3\text{Ni}_2\text{O}_7$ at $T = 290$ K.

D. Fermi surface and magnetic correlations

Next, we calculate the correlated Fermi surfaces [spectral functions $A(\mathbf{k}, \omega)$ evaluated at $\omega = 0$] within DFT + DMFT at $T = 290$ K. In Fig. 5 we show our results for the in-plane FSs for different k_z (for PM LNO with the optimized crystal structure). Our results for the FS of LNO with the experimental (unrelaxed) structure are shown in Fig. S3 of the SM. The DFT + DMFT calculated FSs are similar to that obtained within DFT. In fact, it consists of two electron pockets centered at the Γ and M points of the BZ and one hole pocket at the M point. However, we observe a strong orbital-dependent incoherence of the FS sheets due to correlation effects. Thus, the two electron FS sheets centered at the Γ and M points which are of the mixed Ni x^2-y^2 and $3z^2-r^2$ character show more coherent behavior than the hole pocket at the M point, originating from the Ni $3z^2-r^2$ states. We note that this behavior is in overall agreement with our analysis of the quasiparticle mass enhancements and local spin susceptibility

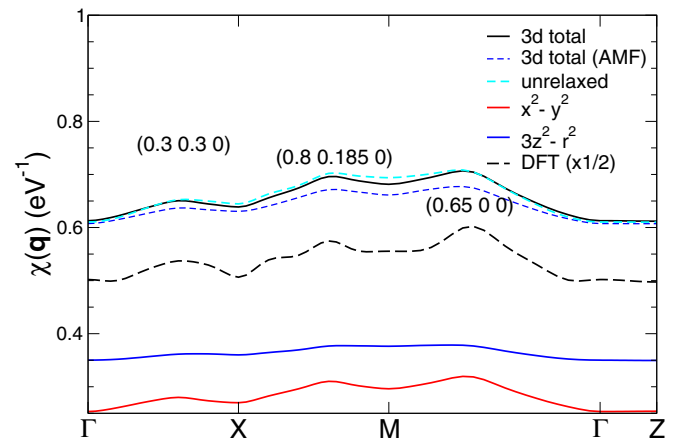


FIG. 5. Orbital resolved static spin susceptibility $\chi(\mathbf{q})$ of the high-pressure PM $\text{La}_3\text{Ni}_2\text{O}_7$ obtained by DFT + DMFT at $T = 290$ K. Our DFT + DMFT results obtained for the around mean-field double counting scheme are depicted as AMF [104].

for the Ni x^2-y^2 and $3z^2-r^2$ orbitals. Moreover, for LNO with the unrelaxed lattice we obtain nearly similar FSs with an additional (coherent) electron FS sheet, centered at the Γ point, of the La $5d$ orbital character. Most interestingly, for $k_z = 0.5$ we note a sizable change of the shape of the electron FS sheet centered at the Z point, caused by the lattice effects, from a square- (for the relaxed) to hexagonlike (for the experimental structure). This is suggestive of the Pomeranchuk instability [110–114], i.e., a change of the FS shape driven by subtle structural effects. Therefore, this suggests that structural effects may be important to understand the electronic behavior of LNO. We conclude that correlation effects mainly result in the orbital-dependent effective mass renormalizations and incoherence of the spectral weight of LNO.

Our results show multiple in-plane nesting of the calculated Fermi surfaces of PM LNO. We therefore proceed with analysis of the symmetry and strength of magnetic correlations in LNO. To this end, we compute the momentum-dependent static magnetic susceptibility $\chi(\mathbf{q})$ in the particle-hole bubble approximation within DFT + DMFT as $\chi(\mathbf{q}) = -k_B T \text{Tr} \sum_{\mathbf{k}, i\omega_n} G_{\mathbf{k}}(i\omega_n) G_{\mathbf{k}+\mathbf{q}}(i\omega_n)$, where $G_{\mathbf{k}}(i\omega_n)$ is the local interacting Green's function for the Ni $3d$ states [115,116].

Our results for different orbital contributions in $\chi(\mathbf{q})$ along the BZ Γ -X-M- Γ -Z path are shown in Fig. 5. For both the DFT and DFT + DMFT results we observe three well-defined maxima of $\chi(\mathbf{q})$ at an incommensurate wave vector (0.3 0.3 0) on the Γ -X branch, (0.8 0.185 0) on the X-M branch, and (0.65 0 0) on the Γ -M branch of the BZ. The first anomaly has the lowest value of $\max[\chi(\mathbf{q})]$ and seems to be associated with an electronic spin density wave instability (with a concomitant charge or bond density wave) characterized by the $(\frac{1}{3} \frac{1}{3} 0)$ modulation of the lattice. The most pronounced instability is associated with the $(\frac{2}{3} 0 0)$ modulation, which is strongly competing with a more complex instability with a wave vector $(\frac{13}{16} \frac{3}{16} 0)$ (according to our interpretation). Our result is in qualitative agreement with the behavior of $\chi(\mathbf{q})$ found in Refs. [65,66], although in both these calculations we note the absence of a broad instability at the X-M direction at $\mathbf{q} = (0.8 0.185 0)$.

Most importantly, recent experimental studies of infinite-layer nickelates $R\text{NiO}_2$ also show the evidence for charge density wave state (or lattice modulations) with a wave vector $(\frac{1}{3} 0 0)$ [46–50]. In addition, the evidence for charge density wave states was previously discussed for the ground state of the hole-doped mixed-valence nickelates (La, Sr) $_2\text{NiO}_4$ (with Sr $x = 1/3$, Ni $^{2.33+}$ ions) and square-planar $\text{La}_4\text{Ni}_3\text{O}_8$ with Ni $^{1.33+}$ and $\text{La}_3\text{Ni}_2\text{O}_6$ with Ni $^{1.5+}$ ions [93–100]. Moreover, for hole-doped $R\text{NiO}_2$ (with a hole-doped Ni $^+$ state) our previous DFT + DMFT calculations suggest the possible for-

mation of bond-disproportionated striped phase with similar behavior [90–92].

Our results suggest complex interplay of spin and charge stripe states, which can be important for understanding the anomalous properties of LNO [46–50,64]. This seems to be consistent with our interpretation of LNO as a negative charge transfer system with the Ni valence state close to 1.75+. Moreover, we note that our DFT + DMFT calculations predict similar $\chi(\mathbf{q})$ for LNO with the experimental structure. This implies that this instability is robust and is essentially unaffected by self-doping effects. This raises the question about the possible role of stripe spin density and charge (or bond) density wave states [117,118] to explain the electronic properties of LNO. This topic calls for further theoretical and experimental studies of the complex interplay between charge order, magnetism, and superconductivity established in nickelate superconductors.

III. CONCLUSION

In conclusion, using the DFT + DMFT method we explore the normal state electronic structure, orbital-selective behavior, Fermi surface topology, and magnetic correlations of the recently discovered double-layer nickelate superconductor $\text{La}_3\text{Ni}_2\text{O}_7$. Based on our results, we propose that LNO is a negative charge transfer mixed-valence material, with the Ni valence state close to 1.75+ (obtained from our analysis of the weights of different atomic configurations of the Ni $3d$ electrons). Our results reveal a remarkable orbital-selective renormalization of the Ni $3d$ bands, with $m^*/m \sim 3$ and 2.3 for the Ni $3z^2-r^2$ and x^2-y^2 orbitals, respectively, in agreement with experimental estimates. Moreover, our results for the k -dependent spectral functions and correlated Fermi surfaces show significant incoherence of the electronic Ni $3z^2-r^2$ states. All these imply the proximity of the Ni $3d$ states to orbital-dependent localization. Our analysis of the momentum-dependent static magnetic susceptibility suggests the possible formation of the spin and charge (or bond) density wave stripe states, which seems to be important for understanding of the anomalous properties of LNO. We propose that superconductivity in double-layer nickelates at high pressure is strongly influenced, or even induced, by in-plane spin fluctuations. Our results suggest the emergence of different stripe states on a microscopic level, in which interplay affects the electronic structure and superconductivity of this material.

ACKNOWLEDGMENTS

We acknowledge support by the Russian Science Foundation Project No. 22-22-00926 [119].

- [1] D. Li, K. Lee, B. Y. Wang, M. Osada, S. Crossley, H. R. Lee, Y. Cui, Y. Hikita, and H. Y. Hwang, Superconductivity in an infinite-layer nickelate, *Nature (London)* **572**, 624 (2019).
 [2] M. Hepting, D. Li, C. Jia, H. Lu, E. Paris, Y. Tseng, X. Feng, M. Osada, E. Been, Y. Hikita *et al.*, Electronic structure of the parent compound of superconducting infinite-layer nickelates, *Nat. Mater.* **19**, 381 (2020).

- [3] S. Zeng, C. S. Tang, X. Yin, C. Li, M. Li, Z. Huang, J. Hu, W. Liu, G. J. Omar, H. Jani, Z. S. Lim, K. Han, D. Wan, P. Yang, S. J. Pennycook, A. T. S. Wee, and A. Ariando, Phase Diagram and Superconducting Dome of Infinite-Layer $\text{Nd}_{1-x}\text{Sr}_x\text{NiO}_2$ Thin Films, *Phys. Rev. Lett.* **125**, 147003 (2020).
 [4] M. Osada, B. Y. Wang, B. H. Goodge, S. P. Harvey, K. Lee, D. Li, L. F. Kourkoutis, and H. Y. Hwang, Nickelate

- superconductivity without rare-earth magnetism: (La, Sr)NiO₂, *Adv. Mater.* **33**, 2104083 (2021).
- [5] B. H. Goodge, D. Li, M. Osada, B. Y. Wang, K. Lee, G. A. Sawatzky, H. Y. Hwang, and L. F. Kourkoutis, Doping evolution of the Mott-Hubbard landscape in infinite-layer nickelates, *Proc. Natl. Acad. Sci. USA* **118**, e2007683118 (2021).
- [6] H. Lu, M. Rossi, A. Nag, M. Osada, D. F. Li, K. Lee, B. Y. Wang, M. Garcia-Fernandez, S. Agrestini, Z. X. Shen, E. M. Been, B. Moritz, T. P. Devereaux, J. Zaanen, H. Y. Hwang, K.-J. Zhou, and W. S. Lee, Magnetic excitations in infinite-layer nickelates, *Science* **373**, 213 (2021).
- [7] N. N. Wang, M. W. Yang, Z. Yang, K. Y. Chen, H. Zhang, Q. H. Zhang, Z. H. Zhu, Y. Uwatoko, L. Gu, X. L. Dong, K. J. Jin, J. P. Sun, and J.-G. Cheng, Pressure-induced monotonic enhancement of T_c to over 30 K in the superconducting Pr_{0.82}Sr_{0.18}NiO₂ thin films, *Nat. Commun.* **13**, 4367 (2022).
- [8] X. Ren, J. Li, W.-C. Chen, Q. Gao, J. J. Sanchez, J. Hales, H. Luo, F. Rodolakis, J. L. McChesney, T. Xiang, J. Hu, F.-C. Zhang, R. Comin, Y. Wang, X. J. Zhou, and Z. Zhu, Strain-induced enhancement of T_c in infinite-layer Pr_{0.8}Sr_{0.2}NiO₂ films, [arXiv:2109.05761](https://arxiv.org/abs/2109.05761).
- [9] G. A. Pan, D. F. Segedin, H. LaBollita, Q. Song, E. M. Nica, B. H. Goodge, A. T. Pierce, S. Doyle, S. Novakov, D. C. Carrizales *et al.*, Superconductivity in a quintuple-layer square-planar nickelate, *Nat. Mater.* **21**, 160 (2022).
- [10] S. Zeng, C. Li, L. E. Chow, Y. Cao, Z. Zhang, C. S. Tang, X. Yin, Z. S. Lim, J. Hu, P. Yang, and A. Ariando, Superconductivity in infinite-layer nickelate La_{1-x}Ca_xNiO₂ thin films, *Sci. Adv.* **8**, ab19927 (2022).
- [11] M. Kitatani, L. Si, O. Janson, R. Arita, Z. Zhong, and K. Held, Nickelate superconductors – a renaissance of the one-band Hubbard model, *npj Quantum Mater.* **5**, 59 (2020).
- [12] H. Chen, A. Hampel, J. Karp, F. Lechermann, and A. J. Millis, Dynamical mean field studies of infinite layer nickelates: Physics results and methodological implications, *Front. Phys.* **10**, 835942 (2022).
- [13] Y. Nomura and R. Arita, Superconductivity in infinite-layer nickelates, *Rep. Prog. Phys.* **85**, 052501 (2022).
- [14] A. S. Botana, K.-W. Lee, M. R. Norman, V. Pardo, and W. E. Pickett, Low valence nickelates: Launching the nickel age of superconductivity, *Front. Phys.* **9**, 813532 (2022).
- [15] Q. Gu and H.-H. Wen, Superconductivity in nickel-based 112 systems, *The Innovation* **3**, 100202 (2022).
- [16] V. I. Anisimov, D. Bukhvalov, and T. M. Rice, Electronic structure of possible nickelate analogs to the cuprates, *Phys. Rev. B* **59**, 7901 (1999).
- [17] K.-W. Lee and W. E. Pickett, Infinite-layer LaNiO₂: Ni¹⁺ is not Cu²⁺, *Phys. Rev. B* **70**, 165109 (2004).
- [18] A. S. Botana and M. R. Norman, Similarities and Differences Between LaNiO₂ and CaCuO₂ and Implications for Superconductivity, *Phys. Rev. X* **10**, 011024 (2020).
- [19] M. Azuma, Z. Hiroi, M. Takano, Y. Bando, and Y. Takeda, Superconductivity at 110 K in the infinite-layer compound (Sr_{1-x}Ca_x)_{1-y}CuO₂, *Nature (London)* **356**, 775 (1992).
- [20] Y. Y. Peng, G. Dellea, M. Minola, M. Conni, A. Amorese, D. Di Castro, G. M. De Luca, K. Kummer, M. Salluzzo, X. Sun, X. J. Zhou, G. Balestrino, M. Le Tacon, B. Keimer, L. Braicovich, N. B. Brookes, and G. Ghiringhelli, Influence of apical oxygen on the extent of in-plane exchange interaction in cuprate superconductors, *Nat. Phys.* **13**, 1201 (2017).
- [21] S. Y. Savrasov and O. K. Andersen, Linear-Response Calculation of the Electron-Phonon Coupling in Doped CaCuO₂, *Phys. Rev. Lett.* **77**, 4430 (1996).
- [22] L. Si, W. Xiao, J. Kaufmann, J. M. Tomczak, Y. Lu, Z. Zhong, and K. Held, Topotactic Hydrogen in Nickelate Superconductors and Akin Infinite-Layer Oxides ABO₂, *Phys. Rev. Lett.* **124**, 166402 (2020).
- [23] P. Werner and S. Hoshino, Nickelate superconductors: Multi-orbital nature and spin freezing, *Phys. Rev. B* **101**, 041104(R) (2020).
- [24] F. Lechermann, Multiorbital Processes Rule the Nd_{1-x}Sr_xNiO₂ Normal State, *Phys. Rev. X* **10**, 041002 (2020).
- [25] J. Karp, A. S. Botana, M. R. Norman, H. Park, M. Zingl, and A. Millis, Many-Body Electronic Structure of NdNiO₂ and CaCuO₂, *Phys. Rev. X* **10**, 021061 (2020).
- [26] J. Karp, A. Hampel, M. Zingl, A. S. Botana, H. Park, M. R. Norman, and A. J. Millis, Comparative many-body study of Pr₄Ni₃O₈ and NdNiO₂, *Phys. Rev. B* **102**, 245130 (2020).
- [27] F. Lechermann, Late transition metal oxides with infinite-layer structure: Nickelates versus cuprates, *Phys. Rev. B* **101**, 081110(R) (2020).
- [28] Y. Wang, C.-J. Kang, H. Miao, and G. Kotliar, Hund's metal physics: From SrNiO₂ to LaNiO₂, *Phys. Rev. B* **102**, 161118(R) (2020).
- [29] Y. Nomura, T. Nomoto, M. Hirayama, and R. Arita, Magnetic exchange coupling in cuprate-analog d^9 nickelates, *Phys. Rev. Res.* **2**, 043144 (2020).
- [30] S. Ryee, H. Yoon, T. J. Kim, M. Y. Jeong, and M. J. Han, Induced Magnetic Two-dimensionality by Hole Doping in Superconducting Nd_{1-x}Sr_xNiO₂, *Phys. Rev. B* **101**, 064513 (2020).
- [31] I. Leonov, S. L. Skornyakov, and S. Y. Savrasov, Lifshitz transition and frustration of magnetic moments in infinite-layer NdNiO₂ upon hole doping, *Phys. Rev. B* **101**, 241108(R) (2020).
- [32] I. Leonov, Effect of lattice strain on the electronic structure and magnetic correlations in infinite-layer (Nd, Sr)NiO₂, *J. Alloys Compd.* **883**, 160888 (2021).
- [33] F. Lechermann, Doping-dependent character and possible magnetic ordering of NdNiO₂, *Phys. Rev. Mater.* **5**, 044803 (2021).
- [34] X. Wan, V. Ivanov, G. Resta, I. Leonov, and S. Y. Savrasov, Exchange interactions and sensitivity of the Ni two-hole spin state to Hund's coupling in doped NdNiO₂, *Phys. Rev. B* **103**, 075123 (2021).
- [35] F. Lechermann, Emergent flat-band physics in $d^{9-\delta}$ multilayer nickelates, *Phys. Rev. B* **105**, 155109 (2022).
- [36] A. L. Kutepov, Electronic structure of LaNiO₂ and CaCuO₂ from self consistent vertex corrected GW approach, *Phys. Rev. B* **104**, 085109 (2021).
- [37] A. Kreisell, B. M. Andersen, A. T. Rømer, I. M. Eremin, and F. Lechermann, Superconducting Instabilities in Strongly Correlated Infinite-Layer Nickelates, *Phys. Rev. Lett.* **129**, 077002 (2022).
- [38] P. Worm, L. Si, M. Kitatani, R. Arita, J. M. Tomczak, and K. Held, Correlations tune the electronic structure of pentalayer

- nickelates into the superconducting regime, *Phys. Rev. Mater.* **6**, L091801 (2022).
- [39] L. Si, P. Worm, D. Chen, and K. Held, Topotactic hydrogen forms chains in ABO₂ nickelate superconductors, *Phys. Rev. B* **107**, 165116 (2023).
- [40] G. L. Pascut, L. Cosovanu, K. Haule, and K. F. Quader, Correlation-temperature phase diagram of prototypical infinite layer rare earth nickelates, *Commun. Phys.* **6**, 45 (2023).
- [41] M. Kitatani, L. Si, P. Worm, J. M. Tomczak, R. Arita, and K. Held, Optimizing Superconductivity: From Cuprates via Nickelates to Palladates, *Phys. Rev. Lett.* **130**, 166002 (2023).
- [42] J. Q. Lin, P. VillarArribi, G. Fabbri, A. S. Botana, D. Meyers, H. Miao, Y. Shen, D. G. Mazzone, J. Feng, S. G. Chiuzbaian, A. Nag, A. C. Walters, M. Garcia-Fernandez, K. J. Zhou, J. Pellicciari, I. Jarrige, J. W. Freeland, J. Zhang, J. F. Mitchell, V. Bisogni, X. Liu, M. R. Norman, and M. P. M. Dean, Strong Superexchange in a d^{9-δ} Nickelate Revealed by Resonant Inelastic X-Ray Scattering, *Phys. Rev. Lett.* **126**, 087001 (2021).
- [43] X. Zhou, X. Zhang, J. Yi, P. Qin, Z. Feng, P. Jiang, Z. Zhong, H. Yan, X. Wang, H. Chen, H. Wu, X. Zhang, Z. Meng, X. Yu, M. B. H. Breese, J. Cao, J. Wang, C. Jiang, and Z. Liu, Antiferromagnetism in Ni-Based Superconductors, *Adv. Mater.* **34**, 2106117 (2022).
- [44] H. Lin, D. J. Gawryluk, Y. M. Klein, S. Huangfu, E. Pomjakushina, F. von Rohr, and A. Schilling, Universal spin-glass behaviour in bulk LaNiO₂, PrNiO₂ and NdNiO₂, *New J. Phys.* **24**, 013022 (2022).
- [45] J. Fowlie, M. Hadjimichael, M. M. Martins, D. Li, M. Osada, B. Y. Wang, K. Lee, Y. Lee, Z. Salman, T. Prokscha, J.-M. Triscone, H. Y. Hwang, and A. Suter, Intrinsic magnetism in superconducting infinite-layer nickelates, *Nat. Phys.* **18**, 1043 (2022).
- [46] M. Rossi, M. Osada, J. Choi, S. Agrestini, D. Jost, Y. Lee, H. Lu, B. Y. Wang, K. Lee, A. Nag, Y.-D. Chuang, C.-T. Kuo, S.-J. Lee, B. Moritz, T. P. Devereaux, Z.-X. Shen, J.-S. Lee, K.-J. Zhou, H. Y. Hwang, and W.-S. Lee, A Broken Translational Symmetry State in an Infinite-Layer Nickelate, *Nat. Phys.* **18**, 869 (2022).
- [47] C. C. Tam, J. Choi, X. Ding, S. Agrestini, A. Nag, B. Huang, H. Luo, M. García-Fernández, L. Qiao, and K.-J. Zhou, Charge density waves in infinite-layer NdNiO₂ nickelates, *Nat. Mater.* **21**, 1116 (2022).
- [48] G. Krieger, L. Martinelli, S. Zeng, L. E. Chow, K. Kummer, R. Arpaia, M. M. Sala, N. B. Brookes, A. Ariando, N. Viart, M. Salluzzo, G. Ghiringhelli, and D. Preziosi, Charge and Spin Order Dichotomy in NdNiO₂ Driven by SrTiO₃ Capping Layer, *Phys. Rev. Lett.* **129**, 027002 (2022).
- [49] X. Ren, R. Sutarto, Q. Gao, Q. Wang, J. Li, Y. Wang, T. Xiang, J. Hu, F.-Ch. Zhang, J. Chang, R. Comin, X. J. Zhou, and Z. Zhu, Symmetry of charge order in infinite-layer nickelates, *arXiv:2303.02865*.
- [50] A. Raji, G. Krieger, N. Viart, D. Preziosi, J.-P. Rueff, and A. Gloter, Charge distribution across capped and uncapped infinite-layer neodymium nickelate thin films, *Small* **2304872** (2023), doi:10.1002/sml.202304872.
- [51] J. Pellicciari, N. Khan, P. Wasik, A. Barbour, Y. Li, Y. Nie, J. M. Tranquada, V. Bisogni, and C. Mazzoli, Comment on newly found Charge Density Waves in infinite layer Nickelates, *arXiv:2306.15086*.
- [52] N. F. Mott, *Metal-Insulator Transitions* (Taylor & Francis, London, 1990).
- [53] M. Imada, A. Fujimori, and Y. Tokura, Metal-insulator transitions, *Rev. Mod. Phys.* **70**, 1039 (1998).
- [54] A. Georges, G. Kotliar, W. Krauth, and M. J. Rozenberg, Dynamical mean-field theory of strongly correlated fermion systems and the limit of infinite dimensions, *Rev. Mod. Phys.* **68**, 13 (1996).
- [55] G. Kotliar, S. Y. Savrasov, K. Haule, V. S. Oudovenko, O. Parcollet, and C. A. Marianetti, Electronic structure calculations with dynamical mean-field theory, *Rev. Mod. Phys.* **78**, 865 (2006).
- [56] P. Sun and G. Kotliar, Extended dynamical mean-field theory and GW method, *Phys. Rev. B* **66**, 085120 (2002).
- [57] S. Biermann, F. Aryasetiawan, and A. Georges, First-Principles Approach to the Electronic Structure of Strongly Correlated Systems: Combining the GW Approximation and Dynamical Mean-Field Theory, *Phys. Rev. Lett.* **90**, 086402 (2003).
- [58] Q. Li, Ch. He, J. Si, X. Zhu, Y. Zhang, and H.-H. Wen, Absence of superconductivity in bulk Nd_{1-x}Sr_xNiO₂, *Commun. Mater.* **1**, 16 (2020).
- [59] B.-X. Wang, H. Zheng, E. Kriviyakina, O. Chmaissem, P. P. Lopes, J. W. Lynn, L. C. Gallington, Y. Ren, S. Rosenkranz, J. F. Mitchell, and D. Phelan, Synthesis and characterization of bulk Nd_{1-x}Sr_xNiO₂ and Nd_{1-x}Sr_xNiO₃, *Phys. Rev. Mater.* **4**, 084409 (2020).
- [60] M. Huo, Z. Liu, H. Sun, L. Li, H. Lui, C. Huang, F. Liang, B. Shen, and M. Wang, Synthesis and properties of La_{1-x}Sr_xNiO₃ and La_{1-x}Sr_xNiO₂, *Chin. Phys. B* **31**, 107401 (2022).
- [61] X. Ding, C. C. Tam, X. Sui, Y. Zhao, M. Xu, J. Choi, H. Leng, J. Zhang, M. Wu, H. Xiao *et al.*, Critical role of hydrogen for superconductivity in nickelates, *Nature (London)* **615**, 50 (2023).
- [62] O. I. Malyi, J. Varignon, and A. Zunger, Bulk NdNiO₂ is thermodynamically unstable with respect to decomposition while hydrogenation reduces the instability and transforms it from metal to insulator, *Phys. Rev. B* **105**, 014106 (2022).
- [63] H. Sun, M. Huo, X. Hu, J. Li, Z. Liu, Y. Han, L. Tang, Z. Mao, P. Yang, B. Wang, J. Cheng, D.-X. Yao, G.-M. Zhang, and M. Wang, Signatures of superconductivity near 80 K in a nickelate under high pressure, *Nature (London)* (2023).
- [64] Z. Liu, H. Sun, M. Huo, X. Ma, Y. Ji, E. Yi, L. Li, H. Liu, J. Yu, Z. Zhang *et al.*, Evidence for charge and spin density waves in single crystals of La₃Ni₂O₇ and La₃Ni₂O₆, *Sci. China Phys. Mech. Astron.* **66**, 217411 (2023).
- [65] Z. Luo, X. Hu, M. Wang, W. Wú, and D.-X. Yao, Bilayer two-orbital model of La₃Ni₂O₇ under pressure, *arXiv:2305.15564*.
- [66] F. Lechermann, J. Gondolf, S. Bötzel, and I. M. Eremin, Electronic correlations and superconducting instability in La₃Ni₂O₇ under high pressure, *arXiv:2306.05121*.
- [67] V. Christiansson, F. Petocchi, and P. Werner, Correlated electronic structure of La₃Ni₂O₇ under pressure, *arXiv:2306.07931*.
- [68] Q.-G. Yang, D. Wang, and Q.-H. Wang, Possible s_±-wave superconductivity in La₃Ni₂O₇, *arXiv:2306.03706*.
- [69] Y. Zhang, L.-F. Lin, A. Moreo, and E. Dagotto, Electronic structure, orbital-selective behavior, and magnetic tendencies in the bilayer nickelate superconductor La₃Ni₂O₇ under pressure, *arXiv:2306.03231*.

- [70] Y. Shen, M. Qin, and G.-M. Zhang, Effective bi-layer model Hamiltonian and density-matrix renormalization group study for the high- T_c superconductivity in $\text{La}_3\text{Ni}_2\text{O}_7$ under high pressure, [arXiv:2306.07837](#).
- [71] Y. Cao and Y.-F. Yang, Flat bands promoted by Hund's rule coupling in the candidate double-layer high-temperature superconductor $\text{La}_3\text{Ni}_2\text{O}_7$, [arXiv:2307.06806](#).
- [72] X. Chen, P. Jiang, J. Li, Z. Zhong, and Y. Lu, Critical charge and spin instabilities in superconducting $\text{La}_3\text{Ni}_2\text{O}_7$, [arXiv:2307.07154](#).
- [73] Z. Liu, M. Huo, J. Li, Q. Li, Y. Liu, Y. Dai, X. Zhou, J. Hao, Y. Lu, M. Wang, and H.-H. Wen, Electronic correlations and energy gap in the bilayer nickelate $\text{La}_3\text{Ni}_2\text{O}_7$, [arXiv:2307.02950](#).
- [74] W. Wú, Z. Luo, D.-X. Yao, and M. Wang, Charge Transfer and Zhang-Rice Singlet Bands in the Nickelate Superconductor $\text{La}_3\text{Ni}_2\text{O}_7$ under Pressure, [arXiv:2307.05662](#).
- [75] J. Hou, P. T. Yang, Z. Y. Liu, J. Y. Li, P. F. Shan, L. Ma, G. Wang, N. N. Wang, H. Z. Guo, J. P. Sun, Y. Uwatoko, M. Wang, G.-M. Zhang, B. S. Wang, and J.-G. Cheng, Emergence of high-temperature superconducting phase in the pressurized $\text{La}_3\text{Ni}_2\text{O}_7$ crystals, [arXiv:2307.09865](#).
- [76] Y.-B. Liu, J.-W. Mei, F. Ye, W.-Q. Chen, and F. Yang, The s_{\pm} -Wave Pairing and the Destructive Role of Apical-Oxygen Deficiencies in $\text{La}_3\text{Ni}_2\text{O}_7$ Under Pressure, [arXiv:2307.10144](#).
- [77] Y. Zhang, D. Su, Y. Huang, H. Sun, M. Huo, Z. Shan, K. Ye, Z. Yang, R. Li, M. Smidman, M. Wang, L. Jiao, and H. Yuan, High-temperature superconductivity with zero-resistance and strange metal behaviour in $\text{La}_3\text{Ni}_2\text{O}_7$, [arXiv:2307.14819](#).
- [78] C. Lu, Z. Pan, F. Yang, and C. Wu, Interlayer coupling driven high-temperature superconductivity in $\text{La}_3\text{Ni}_2\text{O}_7$ under pressure, [arXiv:2307.14965](#).
- [79] K. Haule, Quantum Monte Carlo impurity solver for cluster dynamical mean-field theory and electronic structure calculations with adjustable cluster base, *Phys. Rev. B* **75**, 155113 (2007).
- [80] L. V. Pourovskii, B. Amadon, S. Biermann, and A. Georges, Self-consistency over the charge density in dynamical mean-field theory: A linear muffin-tin implementation and some physical implications, *Phys. Rev. B* **76**, 235101 (2007).
- [81] I. Leonov, A. O. Shorikov, V. I. Anisimov, and I. A. Abrikosov, Emergence of quantum critical charge and spin-state fluctuations near the pressure-induced Mott transition in MnO, FeO, CoO, and NiO, *Phys. Rev. B* **101**, 245144 (2020).
- [82] J. P. Perdew, K. Burke, and M. Ernzerhof, Generalized Gradient Approximation Made Simple, *Phys. Rev. Lett.* **77**, 3865 (1996).
- [83] P. Giannozzi, S. Baroni, N. Bonini, M. Calandra, R. Car, C. Cavazzoni, D. Ceresoli, G. L. Chiarotti, M. Cococcioni, I. Dabo *et al.*, Quantum ESPRESSO: A modular and open-source software project for quantum simulations of materials, *J. Phys.: Condens. Matter* **21**, 395502 (2009).
- [84] P. Giannozzi, O. Andreussi, T. Brumme, O. Bunau, M. B. Nardelli, M. Calandra, R. Car, C. Cavazzoni, D. Ceresoli, M. Cococcioni *et al.*, Advanced capabilities for materials modelling with Quantum ESPRESSO, *J. Phys.: Condens. Matter* **29**, 465901 (2017).
- [85] A. Dal Corso, *Ab initio* phonon dispersions of transition and noble metals: Effects of the exchange and correlation functional, *J. Phys.: Condens. Matter* **25**, 145401 (2013).
- [86] A. Dal Corso, Pseudopotentials periodic table: From H to Pu, *Comput. Mater. Sci.* **95**, 337 (2014).
- [87] The charge transfer energy is estimated as the difference between the energy centers of the Ni $3d$ and O $2p$ bands.
- [88] It is interesting to note that the charge transfer energy estimated taking into account both the occupied and unoccupied parts of the Ni $3d$ and O $2p$ bands as the difference of the first moments of the Green's function of the Ni e_g and O $2p$ states is remarkably smaller, ~ 1.9 eV.
- [89] See Supplemental Material at <http://link.aps.org/supplemental/10.1103/PhysRevB.108.125105> for additional figures with our DFT + DMFT results for LNO with the experimental (unrelaxed) crystal structure.
- [90] K. G. Slobodchikov and I. V. Leonov, Spin density wave, charge density wave, and bond disproportionation wave instabilities in hole-doped infinite-layer RNiO_2 , *Phys. Rev. B* **106**, 165110 (2022).
- [91] Y. Shen, M. Qin, and G.-M. Zhang, Comparative study of charge order in undoped infinite-layer nickelate superconductors, *Phys. Rev. B* **107**, 165103 (2023).
- [92] H. Chen, Y.-F. Yang, and G.-M. Zhang, Charge order from the local Coulomb repulsion in undoped infinite-layer nickelates, [arXiv:2204.12208](#).
- [93] S.-H. Lee and S.-W. Cheong, Melting of Quasi-Two-Dimensional Charge Stripes in $\text{La}_{5/3}\text{Sr}_{1/3}\text{NiO}_4$, *Phys. Rev. Lett.* **79**, 2514 (1997).
- [94] H. Yoshizawa, T. Kakeshita, R. Kajimoto, T. Tanabe, T. Katsufuji, and Y. Tokura, Stripe order at low temperatures in $\text{La}_{2-x}\text{Sr}_x\text{NiO}_4$ with $0.289 < x < 0.5$, *Phys. Rev. B* **61**, R854(R) (2000).
- [95] A. S. Botana, V. Pardo, W. E. Pickett, and M. R. Norman, Charge ordering in $\text{Ni}^{1+}/\text{Ni}^{2+}$ nickelates: $\text{La}_4\text{Ni}_3\text{O}_8$ and $\text{La}_3\text{Ni}_2\text{O}_6$, *Phys. Rev. B* **94**, 081105(R) (2016).
- [96] J. Zhang, Y.-S. Chen, D. Phelan, H. Zheng, M. R. Norman, and J. F. Mitchell, Stacked charge stripes in the quasi-2D trilayer nickelate $\text{La}_4\text{Ni}_3\text{O}_8$, *Proc. Natl. Acad. Sci. USA* **113**, 8945 (2016).
- [97] O. O. Bernal, D. E. MacLaughlin, G. D. Morris, P.-C. Ho, L. Shu, C. Tan, J. Zhang, Z. Ding, K. Huang, and V. V. Poltavets, Charge-stripe order, antiferromagnetism, and spin dynamics in the cuprate-analog nickelate $\text{La}_4\text{Ni}_3\text{O}_8$, *Phys. Rev. B* **100**, 125142 (2019).
- [98] J. Zhang, D. M. Pajerowski, A. S. Botana, H. Zheng, L. Harriger, J. Rodriguez-Rivera, J. P. C. Ruff, N. J. Schreiber, B. Wang, Y.-S. Chen, W. C. Chen, M. R. Norman, S. Rosenkranz, J. F. Mitchell, and D. Phelan, Spin Stripe Order in a Square Planar Trilayer Nickelate, *Phys. Rev. Lett.* **122**, 247201 (2019).
- [99] J. Zhang, D. Phelan, A. S. Botana, Y.-S. Chen, H. Zheng, M. Krogstad, S. G. Wang, Y. Qiu, J. A. Rodriguez-Rivera, R. Osborn, S. Rosenkranz, M. R. Norman, and J. F. Mitchell, Intertwined density waves in a metallic nickelate, *Nat. Commun.* **11**, 6003 (2020).
- [100] J. Hao, X. Fan, Q. Li, X. Zhou, C. He, Y. Dai, B. Xu, X. Zhu, and H.-H. Wen, Charge-stripe fluctuations in $\text{Nd}_4\text{Ni}_3\text{O}_8$ as evidenced by optical spectroscopy, *Phys. Rev. B* **103**, 205120 (2021).

- [101] N. Marzari, A. A. Mostofi, J. R. Yates, I. Souza, and D. Vanderbilt, Maximally localized Wannier functions: Theory and applications, *Rev. Mod. Phys.* **84**, 1419 (2012).
- [102] V. I. Anisimov, D. E. Kondakov, A. V. Kozhevnikov, I. A. Nekrasov, Z. V. Pchelkina, J. W. Allen, S.-K. Mo, H.-D. Kim, P. Metcalf, S. Suga, A. Sekiyama, G. Keller, I. Leonov, X. Ren, and D. Vollhardt, Full orbital calculation scheme for materials with strongly correlated electrons, *Phys. Rev. B* **71**, 125119 (2005).
- [103] E. Gull, A. J. Millis, A. I. Lichtenstein, A. N. Rubtsov, M. Troyer, and P. Werner, Continuous-time Monte Carlo methods for quantum impurity models, *Rev. Mod. Phys.* **83**, 349 (2011).
- [104] In order to check how our results depend on the choice of double counting schemes, we perform the DFT + DMFT calculations using the around mean-field double counting (with the same Hubbard $U = 6$ eV and Hund's exchange $J = 0.95$ eV). We note that this leads to a sizable increase of the quasiparticle mass renormalization, $m^*/m \sim 3.6$ and 4.6 for the Ni $x^2 - y^2$ and $3z^2 - r^2$ orbitals. The instantaneous magnetic moment of Ni ions is $\sim 1.4 \mu_B$. However, we note that our results for the spectral function, Fermi surface, and analysis of static magnetic susceptibility $\chi(\mathbf{q})$ (magnetic correlations) are comparable to that obtained within DFT+DMFT with the fully localized double counting method.
- [105] J. Zaanen, G. A. Sawatzky, and J. W. Allen, Band Gaps and Electronic Structure of Transition-Metal Compounds, *Phys. Rev. Lett.* **55**, 418 (1985).
- [106] T. Mizokawa, H. Namatame, A. Fujimori, K. Akeyama, H. Kondoh, H. Kuroda, and N. Kosugi, Origin of the Band Gap in the Negative Charge-Transfer-Energy Compound NaCuO_2 , *Phys. Rev. Lett.* **67**, 1638 (1991).
- [107] A. Georges, L. de'Medici, and J. Mravlje, Strong Correlations from Hund's Coupling, *Annu. Rev. Condens. Matter Phys.* **4**, 137 (2013).
- [108] L. de'Medici, G. Giovannetti, and M. Capone, Selective Mott Physics as a Key to Iron Superconductors, *Phys. Rev. Lett.* **112**, 177001 (2014).
- [109] In fact, the Ni t_{2g} states appear close to the Fermi level (below -1 eV), are coupled to the Ni e_g states via the (interorbital) Hubbard and Hund's coupling matrix elements, and hence do contribute to the particle-particle scattering process.
- [110] I. Ya. Pomeranchuk, On the stability of a Fermi liquid, *J. Exp. Theor. Phys. (U. S. S. R.)* **3**, 524 (1958).
- [111] I. Ya. Pomeranchuk, On the stability of a Fermi liquid, *Sov. Phys. JETP* **8**, 361 (1959).
- [112] Ch. J. Halboth and W. Metzner, d -Wave Superconductivity and Pomeranchuk Instability in the Two-Dimensional Hubbard Model, *Phys. Rev. Lett.* **85**, 5162 (2000).
- [113] V. Oganesyan, S. A. Kivelson, and E. Fradkin, Quantum theory of a nematic Fermi fluid, *Phys. Rev. B* **64**, 195109 (2001).
- [114] M. Kitatani, N. Tsuji, and H. Aoki, Interplay of Pomeranchuk instability and superconductivity in the two-dimensional repulsive Hubbard model, *Phys. Rev. B* **95**, 075109 (2017).
- [115] S. L. Skornyakov, V. I. Anisimov, D. Vollhardt, and I. Leonov, Effect of electron correlations on the electronic structure and phase stability of FeSe upon lattice expansion, *Phys. Rev. B* **96**, 035137 (2017).
- [116] S. L. Skornyakov, V. I. Anisimov, D. Vollhardt, and I. Leonov, Correlation strength, Lifshitz transition, and the emergence of a two-dimensional to three-dimensional crossover in FeSe under pressure, *Phys. Rev. B* **97**, 115165 (2018).
- [117] J. M. Tranquada, B. J. Sternlieb, J. D. Axe, Y. Nakamura, and S. Uchida, Evidence for stripe correlations of spins and holes in copper oxide superconductors, *Nature (London)* **375**, 561 (1995).
- [118] B. Keimer, S. A. Kivelson, M. R. Norman, S. Uchida, and J. Zaanen, From quantum matter to high-temperature superconductivity in copper oxides, *Nature (London)* **518**, 179 (2015).
- [119] <https://rscf.ru/project/22-22-00926/>.